On the Use of SMAP Soil Moisture for Forecasting NDVI Over CONUS Cropland Regions

Manh-Hung Le[1,2], John D. Bolten[1, *], Kristen M. Whitney[1], David M. Johnson[3], Rick Mueller[3], and Iliana E. Mladenova[4]

[1] Hydrological Sciences Laboratory, NASA Goddard Space Flight Center, Greenbelt MD, USA

[2] Science Applications International Corporation, Greenbelt MD, USA

[3] U.S. Department of Agriculture, National Agricultural Statistics Service, Washington DC, USA

[4] U.S. Department of Agriculture, Foreign Agricultural Service, Washington DC, USA

*Corresponding author: John D. Bolten (john.bolten@nasa.gov)

Key Points:

- SMAP-based root zone soil moisture is a useful predictor for improving NDVI-based crop forecasting.
- Compared to long-term average NDVI, the greatest forecast skill improvements are found in water-limited environments.
- SMAP-based NDVI forecasting demonstrates significant skill in tracking NDVI dynamics during hydrologic disturbances.

Abstract

Vegetation health forecasting (NDVI as a proxy) informs decision-makers about the end of season crop yield productivity but is not well-documented. This study tests improvements in vegetation health forecasting by developing a data-driven Dynamic Agricultural Productivity Indicator (*DAPI*), which simultaneously incorporates satellite-based root zone soil moisture (*RZSM*) and satellite-based NDVI data. *RZSM* is estimated via data assimilation of satellite based SMAP *SM* dataset. We employ the proposed *DAPI* forecast across four cropland types in the CONUS, including corn, cotton, soybeans, and wheat. Results demonstrate superior performance of the *DAPI* forecasts compared to climatology-based NDVI forecasts, with the largest improvements in water-limited regions. DAPI shows particularly good performance during hydrologic disturbances such as floods and droughts. To this end, the *DAPI* approach is useful in estimating future vegetation health for identifying potential food-insecure areas, predicting crop price changes, and projecting expected commodities market trends.

Plain Language Summary

Crop vegetation health can impact crop productivity. Monitoring the dynamics of vegetation health during the growing season informs decision-makers about potential yield productivity. However, research in this area is not well-documented – most crop forecasting models employ stochastic modeling approaches or are based on simple regression of observed NDVI climatology. This study proposes a method to forecast vegetation health by leveraging satellite-based soil moisture, vegetation indices, and a strategic regression approach. We use the NDVI from satellite data as a proxy for vegetation health. Additionally, we utilize NASA Soil Moisture Active Passive (SMAP) satellite data to enhance a water balance model that simulates root zone soil moisture (*RZSM*) in deeper soil layers. We combine *RZSM* with NDVI values to predict NDVI during the growing season at 16-day intervals. Compared to the long-term average NDVI, our NDVI forecasting approach shows the largest improvements in water-limited regions and during extreme events such as floods and droughts.

1 Introduction

The connection between the growth and senescence of vegetation, vegetation greenness, and vegetation health is well established (Zhang et al., 2006). These changes in vegetation dynamics can be quantified through observations in the visible and near infrared spectrum. Normalized Difference Vegetation Index (NDVI), derived from these spectra, estimates the density of green leaves (Tucker, 1979) and is ideal for remotely observing vegetation dynamics, and thus vegetation health.

The prediction of NDVI vegetation dynamics has been a study subject for nearly two decades. These studies have primarily utilized past NDVI values, past climate variables, and environmental factors as predictors. Ji and Peters (2004) is a pioneering effort in NDVI forecasting for Nebraska's grasslands and croplands. The autocorrelation and seasonality within NDVI time series are significant, leading to the widespread use of lagged NDVI values as predictors in vegetation health forecasting models, as documented in numerous studies (Ahmad et al., 2023; Cui et al., 2020; Reddy & Prasad, 2018). It is well understood that vegetation growth is influenced by climate factors such as precipitation, air temperature, humidity, and solar radiation. Incorporating these climate variables has become a common practice in NDVI forecasting (Carreño-Conde et al., 2021; Huang et al., 2017; Wu et al., 2019). Additionally, studies show that including environmental variables such as topographic and vegetation types (Ma et al., 2022), and land cover (Xu et al., 2024) increase NDVI forecasting skills.

Similarly, soil moisture (*SM*) and NDVI have a causal relationship, with the dryness of the soil impacting vegetation health (Bolten et al., 2009; Mladenova et al., 2019), and NDVI aiding in the spatial disaggregation of coarse *SM* (Kim et al., 2017). Evidence suggests that root zone soil moisture (*RZSM*) is a leading indicator of NDVI in monthly cross-correlation analysis (Mladenova et al., 2019). From a physical perspective, water stress during periods of soil moisture deficit can limit photosynthesis via leaf water potential reductions and stomatal closure (Slatyer and Markus, 1968). Plant physiological and biochemical adaptation strategies often show a delayed response to moisture deficit and other environmental stresses, which suggests a "memory" effect in vegetation response (Chaves et al., 2002). Although the relationship between *SM* and NDVI is well-documented, only a few studies have leveraged this lagged relationship to improve vegetation forecasts (Li et al., 2023; Milazzo et al., 2023). Comprehensive

investigations of *SM* as a predictor in forecasting NDVI dynamics over different types of croplands are rather limited to date.

Climatological NDVI is often used as an indicator of NDVI trends for estimating future NDVI projections. For example, the USDA National Agricultural Statistics Service (NASS) is experimenting with the end-of-season crop yield forecasting using the area under the curve of NDVI (Johnson et al., 2021). That is, accumulated NDVI during the growing season is considered a predictor for crop productivity. This approach and the accuracy of the expected at-harvest yield forecasts are contingent upon the accuracy of the NDVI interpolation technique used to forecast the expected NDVI curve and area under the curve. The interpolation typically relies on general knowledge of the crop-specific NDVI behavior throughout the growing season as well as long-term NDVI trend analysis.

This study aims to answer the question: How effective is NDVI forecasting using *SM* compared to climatological NDVI? For this analysis, we used four major crop types across the conterminous U.S. (CONUS): corn, cotton, soybeans, and wheat. We selected these crops because their NDVI dynamics are significantly associated with the end-of-season crop productivity (Johnson, 2016). Whereas previous studies have provided evidence of a relationship between *SM* and the NDVI there still remain questions of the additional skill that is achieved by applying satellite-based soil moisture in the forecasts. This study advances that knowledge by implementing a NDVI forecasting model using *RZSM* via data assimilation of satellite-based SMAP *SM* dataset. To this end, we enhance our understanding of the potential to forecast crop productivity by anticipating the cropland greenness dynamics.

2 Data and Methodology

In our *DAPI* approach, the current NDVI is predicted using lagged NDVI and lagged *RZSM*. The datasets used are presented in Subsection 2.1. The computation of standard rank cross-correlation between NDVI and *RZSM* used to determine the optimal lagged *RZSM* for the

DAPI model is described in Subsection 2.2. The main algorithm development for the *DAPI* is presented in Subsection 2.3, and the forecasting skill assessment is described in Subsection 2.4.

2.1 Data

SMAP, a satellite-based *SM* sensor launched in January 2015 has collected *SM* observations from March 31, 2015 to present (Entekhabi et al., 2010). It combines radar and radiometer images to provide surface *SM* estimates twice daily of the topsoil layer (0–5 cm). The radar failed on July 7, 2015, leading to a reliance on radiometer-only derived *SM* retrievals. Despite this, SMAP SM still achieves its designed soil moisture accuracy of 0.04 m^3/m^3 (Colliander et al., 2017). Strategic application of SMAP *SM* has been shown to improve *RZSM* estimates by providing better physical constraints of soil moisture models (Mladenova et al., 2019).

This study utilized spatially-distributed NASA–USDA Enhanced SMAP *RZSM* time series (0–100 cm) at the 0.1-degree latitude/longitude resolution (~10km) derived by integrating satellite observed SMAP Level 2 *SM* retrievals into the two-layer Palmer water balance model (PM) employed by the USDA Foreign Agricultural Service (FAS) with a 1-D Ensemble Kalman filtering (EnKF) (Bolten, et al., 2009). The SMAP assimilation was specifically designed to improve the accuracy of the USDA FAS *RZSM* information by correcting random errors in modeled estimates associated with poor precipitation forcing (Crow et al., 2012, Bolten & Crow, 2012; Mladenova et al., 2019). In this study, *RZSM* was chosen based on the International Production Assessment Division (IPAD)'s guidance in selecting the appropriate soil moisture profile related to crop growth. Past studies have shown that *RZSM* derived from SMAP data assimilation is effective in properly capturing *RZSM* and NDVI dynamics (Mladenova et al., 2017; 2020).

For a proxy of vegetation health, we used the VIIRS NDVI data provided via the Global Agriculture Monitoring (GLAM) system and generated by the Global Inventory Modeling and Mapping Studies (GIMMS) team at NASA GSFC (Becker-Reshef et al., 2010). Time series of these NDVI products are derived from the Collection 1 VNP09 surface reflectance products with near-real-time eight-day NDVI composites at a 375m spatial resolution globally. Earlier studies show that MODIS and VIIRS NDVI data can be used interchangeably for various applications with uncertainty less than 0.02–0.05 (Skakun et al., 2018).

For crop datasets processing, we integrated crop yield and crop mask datasets from the USDA NASS (USDA NASS, 2016), irrigation information from the Moderate Resolution Imaging Spectroradiometer (MODIS) Irrigated Agriculture Dataset for the United States (MIrAD-US) 250m product (Pervez & Brown, 2010), and county boundaries from the Topologically Integrated Geographic Encoding and Referencing (TIGER) administrative boundary (Marx, 1986). We extracted crop information for four different crop types—corn, cotton, soybeans, and wheat—across the most productive states of CONUS.

Croplands across the CONUS vary from semi-arid regions, where evaporative demand exceeds water supplies in most seasons, to humid regions with adequate water supply for most of the year. That evaporative demand condition is a key factor in identifying drought tolerant crops and agriculture-focused water use strategies, as well as physiological adaptations to water availability (Li et al., 2023; Passioura & Angus, 2010). To reflect this feature, we obtained the aridity index, which is the ratio between long-term precipitation (P) and potential evapotranspiration (PET) (Trabucco & Zomer, 2022). The WorldClim V2.1 climatological datasets (Fick & Hijmans, 2017) were used to provide P and other climate variables needed to derive PET based on the Penman-Monteith equation (Allen et al., 1998). For each crop grid cell, we calculated the average P/PET during the growing seasons from April to November. We classified grid cells into water-limited or energy-limited environments where P/PET was below 0.5 or greater-than-or-equal-to 0.5, respectively (Trabucco & Zomer, 2022).

In Supporting Information S1, we summarize the datasets used in this study (Tab. S1) and provide pre-processing steps (Text S1 and Fig. S1) to integrate information from grid cells for *RZSM*, NDVI, irrigation, and aridity index. These cropland grid cells feature complete 16-day NDVI and RZSM time series during the growing season that spans from Day of Year (DOY) 49 (referred to as DOY049) to DOY289 for the period 2016–2021. To this end, we conducted our experiment to forecast 16-day NDVI at a 0.1-degree resolution. The spatial resolution (0.1 degree) is constrained by the spatial resolution of *RZSM*, while the choice of 16-day forecasting is due to (1) the stronger *RZSM*–NDVI relationship at this temporal scale compared to shorter timescales (e.g., 8-day); (2) the greater availability of NDVI data at 16-day intervals, especially in higher latitudes; and (3) the adequate number of data points for model development.

2.2 Standardized Rank Cross-correlation between *RZSM* and NDVI

We employed standardized rank cross-correlation technique to determine the optimal lag time between *RZSM* and NDVI. That is, DOY composites from all years (DOY049 to DOY289) were grouped according to their specific DOY and ranked relative to each other. The corresponding ranks were then standardized to remove seasonal effects in *RZSM*–NDVI relationships (Crow et al., 2012). The cross-correlation (γ_L) between the standardized ranks for *RZSM* and NDVI with a lagged time L (in 16-day intervals, up to 48-days; Fig. S1 in Supporting Information S1) for each grid was computed as:

$$\gamma_L = \frac{\sum_{t-L}^{N}\left[rank(\mathrm{NDVI})_t - \overline{rank(\mathrm{NDVI})}\right]\left[rank(RZSM)_{t-L} - \overline{rank(RZSM)}\right]}{\sqrt{\sum_{t=L}^{N}\left[rank(\mathrm{NDVI})_t - \overline{rank(\mathrm{NDVI})}\right]^2}\sqrt{\sum_{t=L}^{N}\left[rank(RZSM)_{t-L} - \overline{rank(RZSM)}\right]^2}}, \quad (1)$$

where N is the number of sample data; $rank(\mathrm{NDVI})_t$ is the standardized rank of NDVI at time t; $rank(RZSM)_{t-L}$ is the standardized rank of *RZSM* at the lagged time t-L; and $\overline{rank(\mathrm{NDVI})}$ and $\overline{rank(RZSM)}$ are the time-averaged standardized ranks for a given grid. It is noted that, we initially examined cross-correlation relationship up to 96-day lag (in 16-day intervals) and found that the maximum cross-correlation occurs primarily at the first three lead times (up to 48-day lag). Therefore, to investigate the most significant lead time while preserving data availability for model development, we constrained our cross-correlation analysis to 48 days.

2.3 Dynamic Agricultural Productivity Indicator (DAPI) Approach

We first forecasted 16-day NDVI anomalies and then totaled the forecasted NDVI anomalies to climatological NDVI to yield absolute NDVI values. Climatological NDVI is defined as the long-term average of NDVI values for each DOY, calculated using NDVI data from the period 2012 to 2021.

A multiple linear regression at each NDVI grid cell to forecast NDVI anomalies was developed as follows:

$$\widehat{dNDVI}_{g,t,L} = \alpha_{g,0} + \alpha_{g,1} dNDVI_{g,t-L} + \alpha_{g,2} dSM_{g,t-L_{SM}}, \quad (2)$$

where $\alpha_{g,0}$, $\alpha_{g,1}$, and $\alpha_{g,2}$ are regression constants for grid *g*; *L* is forecasted lead time (in 16-day intervals). $\widehat{dNDVI}_{g,t,L}$ is the forecasted NDVI anomaly for grid *g* at time *t* for lead time *L*;

$NDVI_{g,t-L}$ is NDVI anomalies for grid g at time t-L; $dSM_{g,t-L_{SM}}$ is an anomaly of *RZSM* for grid g at time t-L_{SM}, where L_{SM} is the lagged SM and is selected according to:

$$L_{SM} = \begin{cases} L_{g,opt} \ if \ L \leq L_{g,opt} \\ L \ if \ L > L_{g,opt} \end{cases}, \quad (3)$$

$L_{g,opt}$ is the optimum lagged time for grid g with the highest cross-correlation for grid g between $Rank(NDVI)$ and $Rank(SM)$ defined in Section 2.2, computed as:

$$L_{g,opt} = argmax\{\gamma_L\}, \quad (4)$$

The forecasted absolute NDVI value for grid g at time t for lead time L is calculated based on the climatological NDVI for grid g at time t:

$$\widehat{NDVI}_{g,t,L} = \widehat{dNDVI}_{g,t,L} + NDVI_{g,t,clim}. \quad (5)$$

To evaluate multicollinearity between our two predictors (NDVI anomalies and *RZSM* anomalies), we computed the Variance Inflation Factor (VIF, Daoud 2017) for the entire dataset. The results are summarized in Supplementary Table S3. We did not observe significant correlation between our predictors in the proposed regression models.

Our NDVI forecasting experiment used "leave one out cross validation" (LOOCV) for each year between 2016 to 2021 (James et al., 2013). We used the LOOCV strategy to evaluate how well our model performs on unseen data by leaving one year out from the training dataset. With the assumption that yearly time series are independent of each other, there is minimal impact of this strategy on model performance metrics as we forecast the growing season, all training is within the year. We also consider climatological NDVI (referred to as *CLIM*) as a reference NDVI forecasting model. We employed our DAPI regression on the NASA Center For Climate Simulation (NCCS) system. For automation purposes, regardless of crop type, we divided the total grid cells into ten different subsets and performed the regression model as batch job submissions to the NCCS system. Nearly two hundred thousand regression models were tested with varying running times between 10–12 minutes per job submission.

2.4 Assessment of NDVI Forecasting

We computed the normalized root mean square error (*NRMSE*) to evaluate the forecasting skill, which provides an unbiased performance comparison across different crop types of variable NDVI cycles. *NRMSE* for grid g was calculated according to:

$$RMSE = \sqrt{\frac{1}{n}\sum_{i=1}^{n}\left(NDVI_{g,obs} - NDVI_{g,fcst}\right)^2}, \quad (6)$$

$$std(NDVI_{g,obs}) = \sqrt{\frac{\sum_{i=1}^{n}\left(NDVI_{g,obs,i} - \overline{NDVI}_{g,obs}\right)^2}{n-1}}, \quad (7)$$

$$NRMSE = \frac{RMSE}{std\,(NDVI_{g,obs})}. \quad (8)$$

where $NDVI_{g,obs}$ is the 16-day observed NDVI values and $NDVI_{g,fcst}$ is the 16-day forecasted NDVI values for grid g for a give forecast model $fcst$ ($NDVI_{DAPI}$, or $NDVI_{CLIM}$); n is total sample data; and $std(NDVI_{g,obs})$ is standardized deviation of observed NDVI time series for grid g. *NRMSE* values closer to zero imply a closer fit between forecasted NDVI and observed NDVI. Intercomparison between forecasted NDVI can be assessed by calculating the difference between the proposed forecasting method (e.g., *DAPI*) and the benchmark forecasting method (e.g., *CLIM*) within the same grid cell. A negative difference implies an improvement in the proposed forecasting method.

3 Results

Figure 1 presents the distribution of crop locations and the standardized rank cross-correlations between *RZSM* and NDVI. Water-limited grid cells (aridity index < 0.5) dominate the regions where cotton and wheat are grown, while corn and soybeans are primarily grown in energy-limited environments. Generally, the cross-correlations are higher in water-limited than in energy-limited environments. In water-limited environments, such as arid and semi-arid regions, *RZSM* likely controls vegetation health and coverage, where water is a primary factor influencing vegetation growth (Magagi & Kerr, 2001). From our analysis, in water-limited environments, cotton and wheat exhibit the highest correlations between *RZSM* and NDVI, with median values around 0.5. This is followed by corn and soybeans, with median values around 0.25. In energy-limited environments, these median cross-correlation values within the same crop type are relatively lower than those in water-limited regions, by 0.1 to 0.3.

Comparisons of forecasted NDVI between *CLIM* and three *DAPI* lead times for four crops during 2016–2021 is presented in Figure 2. Compared to *CLIM*, *DAPI* was more skillful at Lead 1 (16-day) and Lead 2 (32-day) for cotton and wheat (Fig. 2b,d). Specifically, median *NRMSE* scores for *CLIM* over cotton and wheat grid cells are 0.953 and 0.958, respectively. For *DAPI* Lead 1, the scores improve to 0.625 (35% improvement) for cotton and 0.611 (37%

234 improvement) for wheat. We also observed improvements of 16.5% for cotton and 16.4% for
235 wheat at *DAPI* Lead 2. For corn and soybeans, the median *NRMSE* scores for *CLIM* are 0.944
236 and 0.943, respectively, with improvements of 17.4% (median *NRMSE* of 0.78) for corn and
237 16.7% (median NRMSE of 0.785) for soybeans at *DAPI* Lead 1. Only slight improvements were
238 noted for *DAPI* Lead 2 over corn and soybean grid cells. Further spatial evaluation (Fig. S3 in
239 Supplementary Information S1) of *DAPI* performance shows geographical distinctions, with
240 *DAPI* skill decreasing from the western to eastern CONUS. This coincides with the linearity
241 strength between *RZSM* and NDVI (Fig. 1c) and the autocorrelation of NDVI itself (Fig. S4 in
242 Supplementary Information S1), with higher cross-correlation and autocorrelation in the western
243 CONUS compared to the eastern CONUS. Aligning with the Fig 2's CDF assessment, we
244 performed a t-test to evaluate whether there is a significant difference between the *NRMSE* of
245 different *DAPI* lead times and the *NRMSE* of *CLIM*. Detailed statistics can be found in Tab. S4
246 in Supplementary Information S1. In conclusion, crops in the western U.S. (where cotton and
247 wheat are dominant) benefit the most from the *DAPI* approach."

248 Hydrologic disturbances such as floods and droughts can significantly impact crop
249 productivity. For instance, extreme precipitation events combined with rapid snowmelt in 2019
250 (Lahmers et al., 2023) resulted in spring flooding that reduced corn productivity in Iowa and
251 soybean productivity in Illinois by -9.6% and -10% respectively compared to the 2016–2021
252 average (USDA NASS, 2024). Conversely, a rainfall deficit in Summer 2020 (Seager et al.,
253 2022) in Northeast Texas led to a -2.65% decrease in cotton productivity (USDA NASS, 2024).
254 Wheat productivity in Kansas in 2018 was exceptionally low, 21.9% below the 2016–2021
255 average (USDA NASS, 2024), likely due to a rainfall deficit-induced exceptional spring drought
256 (Unrein, 2019). We specifically examine the dynamics of observed NDVI and different NDVI
257 forecasting models for these hydrologic disturbances in Iowa (for corn NDVI forecasting), Texas
258 (cotton), Illinois (soybeans), and Kansas (wheat) (Fig. 3). Generally, during hydrologic
259 disturbances, we observed that *DAPI* is skillful at two lead times, with a larger portion of skill
260 improvement (negative difference between $NRMSE_{DAPI}$ and $NRMSE_{CLIM}$) across the studied
261 counties in red-code colors (ratio counties with red-coded colors are greater than 60%).

262 This is because, during the disturbance years, observed NDVI significantly deviates from
263 $NDVI_{CLIM}$, and NDVI forecasting appears to better track these deviations (Fig. 4). For example,
264 corn and soybeans in 2019 had delayed planting times due to wet soil conditions in the Midwest

(Johnson et al., 2021; Lahmers et al., 2023), so that a smaller and later peak has been observed for the temporal NDVI of corn and soybeans in 2019. Observed NDVI for cotton was much lower compared to $NDVI_{CLIM}$, especially during the summer. Wheat NDVI dynamics were lower than $NDVI_{CLIM}$ in the spring but higher during the rest of the growing season. These abnormal variations resulted in higher error for the $NDVI_{CLIM}$, with *NRMSE* scores between 0.37–0.97. With the *DAPI* approach, performance improved significantly for Lead 1, with an average reduction of *NRMSE* by 20% and 8.3% for Lead 2. We also analyzed normal years (data not shown) and detected moderately improved forecasting skill from the *DAPI* approach in those years. In conclusion, NDVI timing is highly variable relative to $NDVI_{CLIM}$ during disturbance conditions, where the *DAPI* approach can better track NDVI timing.

4 Discussion

We isolated the impact of *SM* in our *DAPI* approach by implementing a version of *DAPI* without the *RZSM* term in Eq. (2). Intercomparison between *DAPI* with and without *SM*, we observed improvement of *DAPI* with *SM* at 72.5% grid cells for Lead 1 across the studied domain (Fig. S5a in Supplementary Information S1). With Lead 2 and Lead 3, the total improved grid cells for models using *SM* are reduced, accounting for 39.8% and 14.5% of the total grid cells, respectively (Fig. S5b and Fig. S5c). As expected, geographical patterns are distinct, with more areas in the western CONUS showing benefits from including soil moisture. Future studies could quantify how the importance of *SM* changes over lead time affects its application to different real-world NDVI prediction scenarios. SMAP-based *RZSM* may be more sensitive to extreme hydrological disturbances than moderate events. The newly developed added-value of SMAP-based products, such as the Flash Drought Stress Index (FDSI, Sehgal et al., 2021), which is sensitive to rapid flash-drought disturbances, could be a potential predictor to enhance the capabilities of the SMAP-based *DAPI* for forecasting vegetation health during hydrological disturbances.

Nearly half of the studied grid cells contain multiple crops due to the coarse spatial resolution of our experimental design (Fig. S6a in Supplementary Information S1). This introduces noise into the observed NDVI and subsequently affects *DAPI* forecasting, as it mixes vegetation growth signals from different crop behaviors. We investigated whether there was a difference in NDVI forecasting skill between multiple-crop grid cells and single-crop grid cells.

For this, we identified the closest single-crop grid cells to each multiple-crops grid cell as control points and computed the difference in *NRMSE* values between the multiple-crops and single-crop grid cells for each pair ($NRMSE_{multiple\ crop} - NRMSE_{single\ crop}$). Boxplot distributions (Fig. S6) indicate no significant difference in forecasting skill in NRMSE over multiple crops compared to the single crop grid cells ($p<0.01$, t-test mean difference assessment). These analyses demonstrate our model's robustness across grid cells with mixed crops.

We further evaluated the impact of irrigation on our forecasting model performances (Fig. S7 in Supplementary Information S1) as irrigation practices appear to impact SMAP *SM* signals (Jalilvand et al., 2023; Lawston et al., 2017), and consequent *RZSM* estimates. We identified the closest rainfed grid cells to each irrigated grid cell as control points and computed the difference in *NRMSE* values between the irrigated and control grid cells for each pair ($NRMSE_{Irrigated}$ - $NRMSE_{Rainfed}$). Boxplot distributions indicate a significant increase in *NRMSE* over irrigated areas compared to the rainfed grid cells ($p<0.01$, t-test mean difference assessment).

Further studies could consider using SMAP L4 (Reichle et al., 2022) instead of NASA-USDA Enhanced SMAP, as this product shows accurate *RZSM* in current studies (Hoylman et al., 2024). In addition, it is now updated in near real-time on Google Earth Engine (GEE), which could make our SM-based DAPI operational vegetation health forecasting feasible on open platforms like GEE. High-spatial-resolution NDVI forecasting is considered for future investigation. Although the somewhat coarse 0.1-degree resolution is useful for county-level crop assessments (Fig.3 and Fig.4), it is not be practical for field-scale applications. The current algorithm development could apply downscaled SMAP observations from 0.1 degree to 0.01 degree (Fang et al., 2024; Liu et al., 2022). Therefore, utilizing such high-resolution *RZSM* to develop NDVI forecasting models could have more impact on field-scale analysis and reduce forecasting uncertainties due to mixing crop signals.

Another avenue for future study is to explore machine learning and artificial intelligence algorithms to better model non-linear relationships in the NDVI forecasted framework (Ma et al., 2022). For example, we could train a deep learning model across all crop grid cells to better utilize big data at both spatial and temporal scales. Additional SMAP-related products, such as water table data derived from SMAP-based shallow groundwater detection algorithms (Soylu

and Bras, 2021) could also be included to improve the DAPI approach's performances over irrigated crop land areas.

5 Conclusions

To better support operational USDA NASS in utilizing remotely sensed NDVI in agricultural applications, this study developed a soil moisture-based Dynamic Agricultural Productivity Indicator (*DAPI*) to forecast NDVI over four major croplands in CONUS. We highlight the potential of *RZSM*, derived from SMAP-based Water Balance Data Assimilation, as a valuable predictor. Compared to climatological NDVI (*CLIM*), our *DAPI* approach improves NDVI forecasting (in 16-day intervals) by 35% and 37% for Lead 1 and 16.5% and 16.4% for Lead 2 for cotton and wheat, respectively. For corn and soybeans, the *DAPI* approach outperforms *CLIM* at Lead 1 with improvements of 17.4% and 16.7%, respectively. During years with disturbances such as floods and droughts, the benefits of *DAPI* were more apparent, showing advantages for at least two lead times. We provide evidence that *DAPI* is promising as a data-driven model for predicting future vegetation greenness, which is envisaged to support quantifying crop productivity at the end of season.

Open Research

SMAP-based *RZSM* Palmer water balance model dataset was obtained from Google Earth Engine (https://developers.google.com/earth-engine/datasets/catalog/NASA_USDA_HSL_SMAP10KM_soil_moisture#description). VIIRS NDVI was obtained from the Global Inventory Modeling and Mapping Studies (GIMMS) Global Agricultural Monitoring at https://gimms.gsfc.nasa.gov/. Crop mask data were obtained from the USDA NASS at https://www.nass.usda.gov/Research_and_Science/Cropland/Release/index.php, while crop yield data were accessed through R software and the rnassqs package (https://github.com/ropensci/rnassqs) (Potter, 2019). The Moderate Resolution Imaging Spectroradiometer (MODIS) Irrigated Agriculture Dataset for the United States (MIrAD-US) is obtained from Brown et al., 2019. Aridity Index data is obtained from Zomer and Trabucco, 2019. U.S. county boundaries are obtained from https://www.census.gov/geographies/mapping-files/time-series/geo/tiger-line-file.html.

Acknowledgments

The authors would like to express our gratitude to the SMAP Science Team for their funding support. We thank the NASA Center for Climate Simulation (NCCS) system for providing the HPC resources that enabled modeling implementation in this study. We also acknowledge the early contributions of Dr. Nazmus Sazib and Dr. Tasnuva Rouf and the proofreading of the initial manuscript version by Dr. Vasana Dharmadasa.

References

Ahmad, R., Yang, B., Ettlin, G., Berger, A., & Rodríguez-Bocca, P. (2023). A machine-learning based ConvLSTM architecture for NDVI forecasting. *International Transactions in Operational Research*, 30(4): 2025-2048. https://doi.org/10.1111/itor.12887

Allen, R.G., Pereira, L.S., Raes, D., & Smith, M. (1998). Crop evapotranspiration-Guidelines for computing crop water requirements-FAO Irrigation and drainage paper 56. *Fao, Rome,* 300(9), D05109.

Becker-Reshef, I., Justice, C., Sullivan, M., Vermote, E., Tucker, C., Anyamba, A., Small, J., Pak, E., Masuoka, E., Schmaltz, J., Hanson, M., Pittman, K., Birkett, C., Williams, D., Reynolds, C., & Doorn, B. (2010). Monitoring Global Croplands with Coarse Resolution Earth Observations: The Global Agriculture Monitoring (GLAM) Project. *Remote Sensing, 2*, 1589-1609. https://doi.org/10.3390/rs2061589

Bolten, J.D., & Crow, W.T. (2012). Improved prediction of quasi-global vegetation conditions using remotely-sensed surface soil moisture. *Geophysical Research Letters*, 39(19). https://doi.org/10.1029/2012GL053470

Bolten, J.D., Crow, W.T., Zhan, X., Jackson, T.J., & Reynolds, C.A. (2009). Evaluating the utility of remotely sensed soil moisture retrievals for operational agricultural drought monitoring. *IEEE Journal of Selected Topics in Applied Earth Observations and Remote Sensing*, 3(1): 57-66. https://doi.org/10.1109/JSTARS.2009.2037163

Brown, J.F., Howard, D.M., Shrestha, D., & Benedict, T.D., (2019). Moderate Resolution Imaging Spectroradiometer (MODIS) Irrigated Agriculture Datasets for the Conterminous United States (MIrAD-US). [Dataset]. U.S. Geological Survey data release. https://doi.org/10.5066/P9NA3EO8.

Carreño-Conde, F., Sipols, A.E., de Blas, C.S., & Mostaza-Colado, D. (2021). A forecast model applied to monitor crops dynamics using vegetation indices (NDVI). *Applied Sciences*, 11(4): 1859. https://doi.org/10.3390/app11041859

Chaves, M.M., Pereira, J.S., Maroco, J., Rodriques, M.L.,Ricardo, C. P. P., Osório, M.L., Carvalho, I. , Faria, T., & Pinheiro, C. (2002). How plants cope with water stress in the field? Photosynthesis and growth. *Annals of Botany*, 89(7): 907. https://doi.org/10.1093/aob/mcf105

Colliander, A., Jackson, T.J., Bindlish, R., Chan, S., Das, N., Kim, S.B., Cosh, M.H., Dunbar, R.S., Dang, L., Pashaian, L., Asanuma, J., Aida, K., Berg, A., Rowlandson, T., Bosch, D., Caldwell, T., Caylor, K., Goodrich, D., al Jassar, H., Lopez-Baeza, E., Martínez-Fernández, J., González-Zamora, A., Livingston, S., McNairn, H., Pacheco, A., Moghaddam, M., Montzka, C., Notarnicola, C., Niedrist, G., Pellarin, T., Prueger, J., Pulliainen, J., Rautiainen, K., Ramos, J., Seyfried, M., Starks, P., Su, Z., Zeng, Y., van der Velde, R., Thibeault, M., Dorigo, W., Vreugdenhil, M., Walker, J.P., Wu, X., Monerris, A., O'Neill, P.E., Entekhabi, D., Njoku, E.G., & Yueh, S. (2017). Validation of SMAP surface soil moisture products with core validation sites. *Remote Sensing of Environment*, 191, 215-231, 0034-4257. https://doi.org/10.1016/j.rse.2017.01.021

Crow, W.T., Kumar, S.V., & Bolten, J.D. (2012). On the utility of land surface models for agricultural drought monitoring. *Hydrology and Earth System Sciences*, 16(9): 3451-3460. https://doi.org/10.5194/hess-16-3451-2012, 2012.

Cui, C., Zhang, W., Hong, Z., & Meng, L. (2020). Forecasting NDVI in multiple complex areas using neural network techniques combined feature engineering. *International Journal of Digital Earth*, 13(12): 1733-1749. https://doi.org/10.1080/17538947.2020.1808718

Daoud, J. I. (2017). Multicollinearity and regression analysis, *IOP Publishing*, https://doi.org/10.1088/1742-6596/949/1/012009

Entekhabi, D., Njoku, E. G., O'neill, P. E., Kellogg, K. H., Crow, W. T., Edelstein, W. N., Entin J.K, Goodman S. D., Jackson T.J., Johnson J., Kimball J., Piepmeier J.R., Koster R.D., Martin N., McDonald K.C., Moghddam M., Moran S., Reichle R., Shi J.C., Spencer M.W., Thurman S. W., Tsang L., & Van Zyl, J. (2010). The soil moisture active passive (SMAP) mission. *Proceedings of the IEEE*, 98(5), 704-716. https://doi.org/10.1109/JPROC.2010.2043918.

Fick, S.E., & Hijmans, R.J. (2017). WorldClim 2: new 1-km spatial resolution climate surfaces for global land areas. *International Journal of Climatology*, 37(12): 4302-4315. https://doi.org/10.1002/joc.5086

Fang, B., Lakshmi, V., & Zhang, R. (2024). Validation of downscaled 1-km SMOS and SMAP soil moisture data in 2010–2021. *Vadose Zone Journal*, 23, e20305. https://doi.org/10.1002/vzj2.20305

Hoylman, Z. H., Holden, Z., Bocinsky, R. K., Ketchum, D., Swanson, A., & Jencso, K. (2024). Optimizing drought assessment for soil moisture deficits. Water Resources Research, 60(6), e2023WR036087. https://doi.org/10.1029/2023WR036087

Huang, S., Ming, B., Huang, Q., Leng, G., & Hou, B. (2017). A case study on a combination NDVI forecasting model based on the entropy weight method. *Water Resources Management*, 31: 3667-3681. https://doi.org/10.1007/s11269-017-1692-8

Jalilvand, E., Abolafia-Rosenzweig, R., Tajrishy, M., Kumar, S. V., Mohammadi, M. R., & Das, N. N. (2023). Is It Possible to Quantify Irrigation Water-Use by Assimilating a High-Resolution Satellite Soil Moisture Product?. *Water Resources Research*, 59(4), e2022WR033342. https://doi.org/10.1029/2022WR033342

James, G., Witten, D., Hastie, T., & Tibshirani, R. (2013). An introduction to statistical learning, 112. *Springer*. https://doi.org/10.1007/978-1-0716-1418-1

Ji, L., & Peters, A.J. (2004). Forecasting vegetation greenness with satellite and climate data. *IEEE Geoscience and Remote Sensing Letters*, 1(1): 3-6. https://doi.org/10.1109/LGRS.2003.821264

Johnson, D.M. (2016). A comprehensive assessment of the correlations between field crop yields and commonly used MODIS products. *International Journal of Applied Earth Observation and Geoinformation*, 52: 65-81. https://doi.org/10.1016/j.jag.2016.05.010

Johnson, D.M.; Rosales, A.; Mueller, R.; Reynolds, C.; Frantz, R.; Anyamba, A.; Pak, E.; & Tucker, C. (2021). USA Crop Yield Estimation with MODIS NDVI: Are Remotely Sensed Models Better than Simple Trend Analyses? *Remote Sensing 13*, 4227. https://doi.org/10.3390/rs13214227

Kim, S., Balakrishnan, K., Liu, Y., Johnson, F., & Sharma, A. (2017). Spatial disaggregation of coarse soil moisture data by using high-resolution remotely sensed vegetation products. *IEEE Geoscience and Remote Sensing Letters, 14(9): 1604-1608*. https://doi.org/10.1109/LGRS.2017.2725945

Kumar, S.V., Peters-Lidard C.D., Tian Y., Houser P.R., Geiger J., Olden S., Lighty L., Eastman J.L., Doty B., Dirmeyer P., Adams J., Mitchell K., Wood E.F., & Sheffield J. (2006). Land Information System - An interoperable framework for high resolution land surface modeling. *Environmental Modeling & Software*, 21, 1402-1415. https://doi.org/10.1016/j.envsoft.2005.07.004

Lahmers, T.M., Kumar, S.V., Locke, K.A., Wang, S., Getriana, A., Wrzesien, M., Liu, P., & Ahmad, S.K. (2023). Interconnected hydrologic extreme drivers and impacts depicted by remote sensing data assimilation. *Science Report 13, 3*411. https://doi.org/10.1038/s41598-023-30484-4

Lawston, P.M., Santanello Jr, J.A., & Kumar, S.V. (2017). Irrigation signals detected from SMAP soil moisture retrievals. *Geophysical Research Letters*, 44(23): 11-860. https://doi.org/10.1002/2017GL075733

Li, Y., van Dijk, A.I.J.M., Tian, S., & Renzullo, L.J. (2023). Skill and lead time of vegetation drought impact forecasts based on soil moisture observations. *Journal of Hydrology*, 620: 129420. https://doi.org/10.1016/j.jhydrol.2023.129420

Liu, P.-W., Bindlish R., O'Neill, P., Fang, B., Lakshmi, V., Yang, Z., Cosh, M.H., Bongiovanni, T., Collins, C.H., Starks, P.J., Prueger, J., Bosch, D.D., Seyfried, M., & Williams, M.R. (2022). Thermal hydraulic disaggregation of SMAP soil moisture over the continental United States. *IEEE Journal of Selected Topics in Applied Earth Observations and Remote Sensing*, 15: 4072-4092. https://doi.org/10.1109/JSTARS.2022.3165644

Ma, Y., Hu, Y., Moncrieff, G. R., Slingsby, J. A., Wilson, A. M., Maitner, B., & Zhou, R. Z. (2022). Forecasting vegetation dynamics in an open ecosystem by integrating deep learning and environmental variables. *International Journal of Applied Earth Observation and Geoinformation*, 114, 103060. https://doi.org/10.1016/j.jag.2022.103060

Magagi, R.D., & Kerr, Y.H. (2001). Estimating surface soil moisture and soil roughness over semiarid areas from the use of the copolarization ratio. *Remote Sensing of Environment,* 75(3): 432-445. https://doi.org/10.1016/S0034-4257(00)00185-1

Marx, R.W., 1986. The TIGER system: Automating the geographic structure of the United States census. *Government Publications Review*, 1713(2): 181-201. https://doi.org/10.1016/0277-9390(86)90003-8

Milazzo, F., Brocca, L., & Vanwalleghem, T. (2024). NDVI Prediction of Mediterranean Permanent Grasslands Using Soil Moisture Products. *Agronomy*, 14(8), 1798. https://doi.org/10.3390/agronomy14081798

Mladenova, I. E., Bolten J. D., Crow W. T., Anderson M. C., Hain C. R., Johnson D. M., & Mueller R. (2017). Intercomparison of soil moisture, evaporative stress, and vegetation indices for estimating corn and soybean yields over the US, *IEEE Journal of Selected Topics in Applied Earth Observations and Remote Sensing*, 10(4), 1328-1343. https://doi.org/10.1109/JSTARS.2016.2639338

Mladenova, I. E., Bolten, J. D., Crow, W. T., Sazib, N., Cosh, M. H., Tucker, C. J., & Reynolds, C. (2019). Evaluating the operational application of SMAP for global agricultural drought monitoring. *IEEE Journal of Selected Topics in Applied Earth Observations and Remote Sensing*, 12(9), 3387-3397. https://doi.org/10.1109/Jstars.2019.2923555

Mladenova, I. E., Bolten J. D., Crow W., Sazib N., & Reynolds C.(2020). Agricultural drought monitoring via the assimilation of SMAP soil moisture retrievals into a global soil water balance model. *Frontiers in Big Data*, 3, 10. https://doi.org/10.3389/fdata.2020.00010

Passioura, J.B., & Angus, J.F. (2010). Improving productivity of crops in water-limited environments. *Advances in Agronomy*, 106: 37-75. https://doi.org/10.1016/S0065-2113(10)06002-5

Pervez, M.S., & Brown, J.F. (2010). Mapping irrigated lands at 250-m scale by merging MODIS data and national agricultural statistics. *Remote Sensing*, 2(10): 2388-2412. https://doi.org/10.3390/rs2102388

Potter N. A. (2019). ropensci/rnassqs: Ag Land, Incl Buildings - Revised (v0.6.1). [Software]. Zenodo. https://doi.org/10.5281/zenodo.3532167

Reddy, D.S., & Prasad, P.R.C. (2018). Prediction of vegetation dynamics using NDVI time series data and LSTM. *Modeling Earth Systems and Environment*, 4: 409-419. https://doi.org/10.1007/s40808-018-0431-3

Reichle, R., De Lannoy, G., Koster, R. D., Crow, W. T., Kimball, J. S., Liu, Q., & Bechtold, M. (2022). SMAP L4 Global 3-hourly 9 km EASE-Grid Surface and Root Zone Soil Moisture Analysis Update, Version 7, Boulder, Colorado USA. [Dataset]. NASA National Snow and Ice Data Center Distributed Active Archive Center. https://10.5067/LWJ6TF5SZRG3

Seager, R., Ting M., Alexander P., Nakamura J., Liu H., Li C., and Simpson I. R. (2022). Mechanisms of a meteorological drought onset: Summer 2020 to spring 2021 in southwestern North America. *Journal of Climate*, 35(22): 7367-7385. https://doi.org/10.1175/JCLI-D-22-0314.1

Sehgal, V., Gaur N., & Mohanty B. P. (2021). Global flash drought monitoring using surface soil moisture. *Water Resources Research*, 57(9), e2021WR029901. https://doi.org/10.1029/2021WR029901

Soylu, M. E., & Bras. R. L. (2021). Detecting shallow groundwater from spaceborne soil moisture observations. *Water Resources Research*, 57(2), e2020WR029102. https://doi.org/10.1029/2020WR029102

Skakun, S., Justice, C.O., Vermote, E., Roger, J.-C. (2018). Transitioning from MODIS to VIIRS: an analysis of inter-consistency of NDVI data sets for agricultural monitoring. *International Journal of Remote Sensing*, 39(4): 971-992. https://doi.org/10.1080/01431161.2017.1395970

Slatyer, R.O., & Markus, D.K. (1968). Plant-water relationships. Soil science, 106(6): 478.

Trabucco, A., & Zomer, R. (2022). Version 3 of the Global Aridity Index and Potential Evapotranspiration Database. Climate Database v22019(9): 409. https://doi.org/10.1038/s41597-022-01493-1

Tucker, C.J. (1979). Red and photographic infrared linear combinations for monitoring vegetation. *Remote sensing of Environment*, 8(2): 127-150.https://doi.org/10.1016/0034-4257(79)90013-0

Unrein, A.H. (2019). Hydrologic conditions in Kansas, water year 2018. 2327-6932, *US Geological Survey*. https://doi.org/10.3133/fs20193042

USDA NASS (2016). USDA national agricultural statistics service cropland data layer. Available online: https://www.nass.usda.gov/Research_and_Science/Cropland/Release/index.php. In: USDA-NASS, W., DC (Ed.).

USDA NASS (2024). Quick Stats. Available online: https://www.nass.usda.gov/Quick_Stats. USDA.

Wu, T., Fu, H., Feng, F., & Bai, H. (2019). A new approach to predict normalized difference vegetation index using time-delay neural network in the arid and semi-arid grassland. *International Journal of Remote Sensing*, 40(23): 9050-9063. https://doi.org/10.1080/01431161.2019.1624870

Xu, L., Cai, R., Yu, H., Du, W., Chen, Z., & Chen, N. (2024). Monthly NDVI prediction using spatial autocorrelation and nonlocal attention networks. *IEEE Journal of Selected Topics in Applied Earth Observations and Remote Sensing*. https://doi.org/10.1109/JSTARS.2024.3350053

Zhang, X., Friedl, M.A., & Schaaf, C.B. (2006). Global vegetation phenology from Moderate Resolution Imaging Spectroradiometer (MODIS): Evaluation of global patterns and comparison with in situ measurements. *Journal of Geophysical Research: Biogeoscience*s, 111(G4). https://doi.org/10.1029/2006JG000217

Zomer, R., & Trabucco, A. (2019). Global Aridity Index and Potential Evapotranspiration (ET0) Database: Version 3. [Dataset]. Figshare. https://doi.org/10.6084/m9.figshare.7504448.v6

516 FIGURES

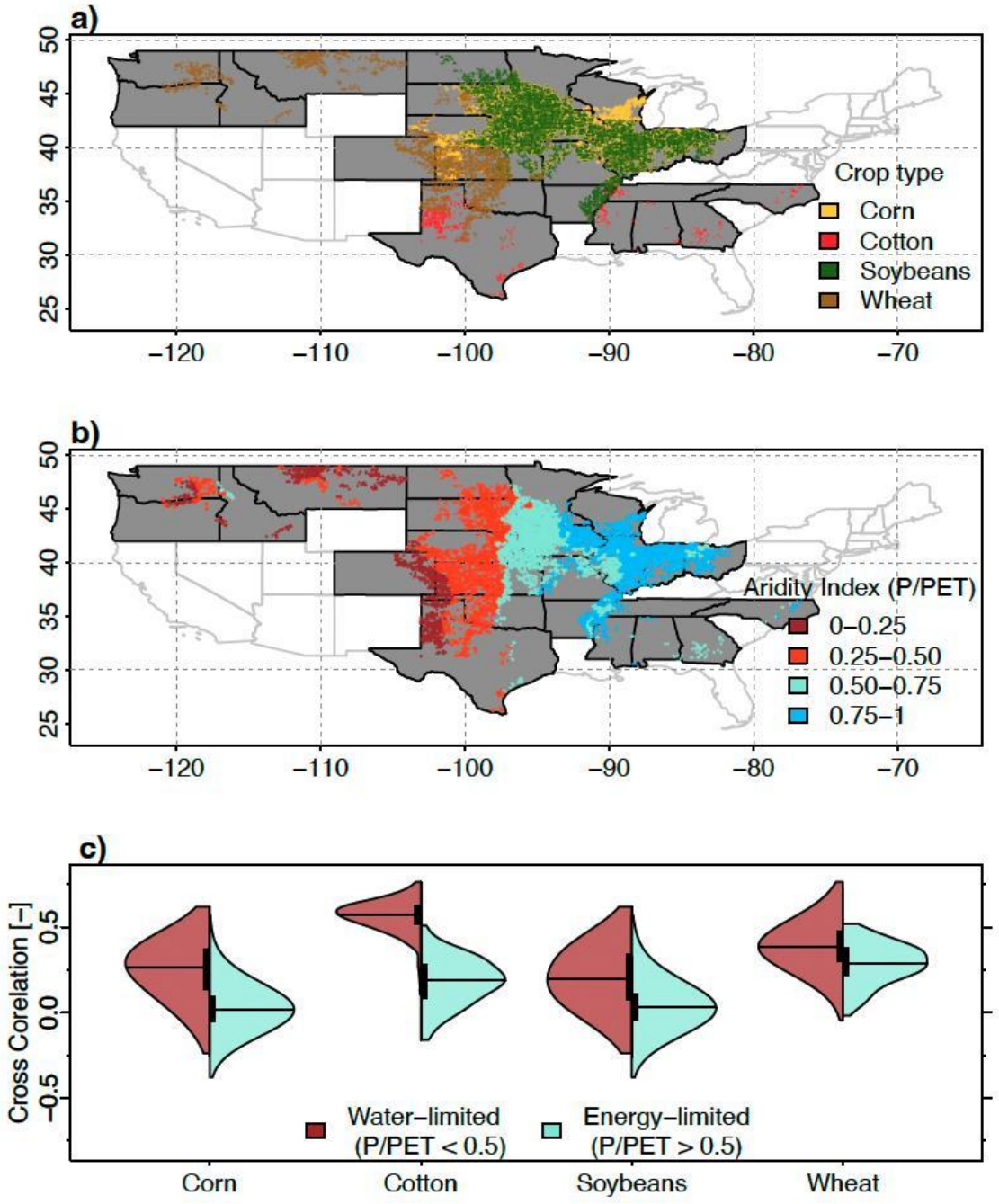

517

518 **Figure 1.** Distribution of (a) crop locations for corn, cotton, soybeans, and wheat; (b) aridity
519 index across the crop grid cells, and (c) split plot of maximum cross-correlation between
520 standard rank *RZSM* and standard rank NDVI for each crop type based on water-limited and
521 energy-limited environments. A grid cell is classified as "water-limited" if its long-term P/PET is
522 less than 0.5, and as "energy-limited" if P/PET is greater than 0.5.

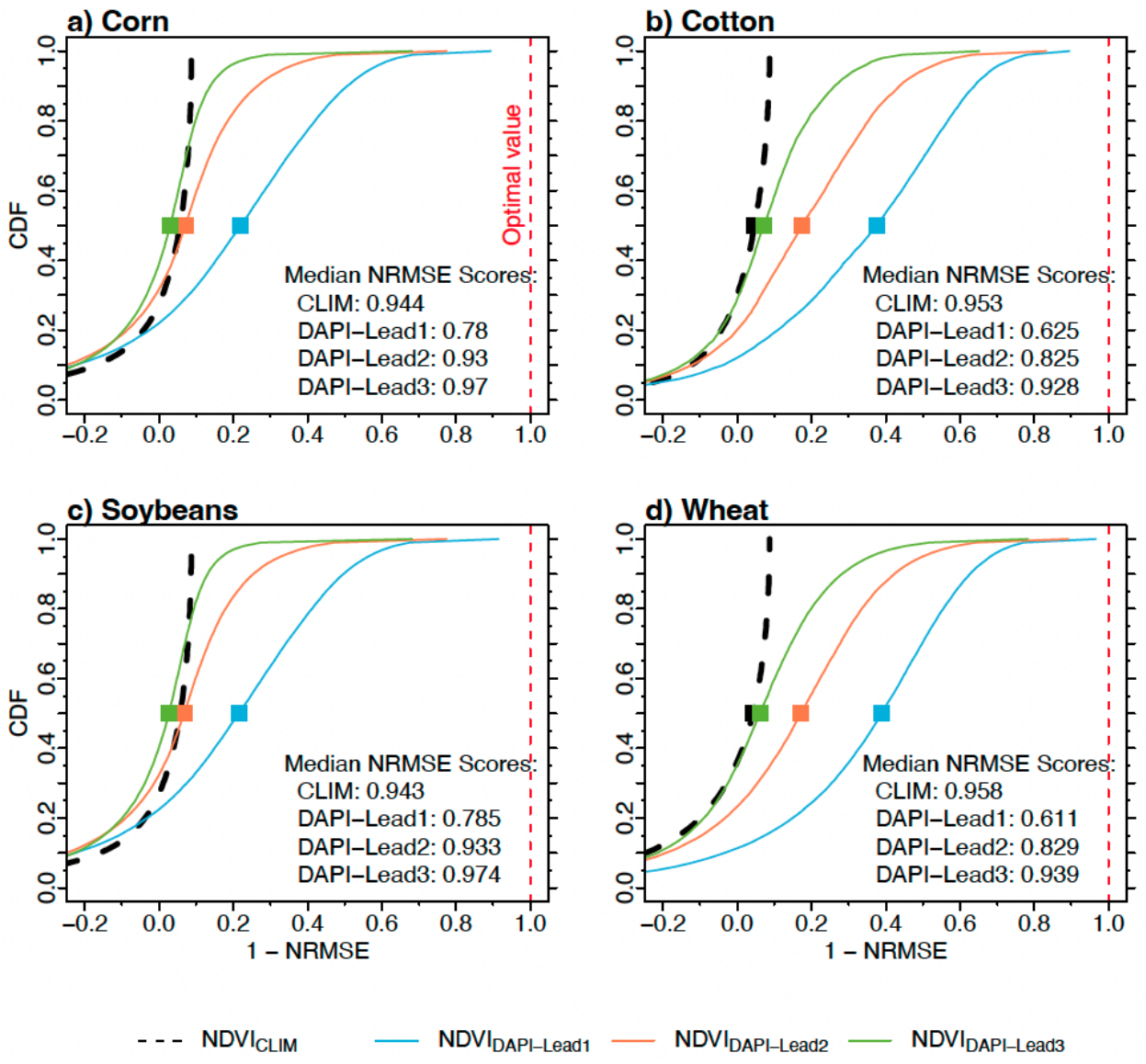

Figure 2. Aggregate NDVI forecasting performances from 2016 to 2021, in terms of (a) Corn, (b) Cotton, (c) Soybeans, and (d) Wheat, for the *CLIM* model (dashed black line) and three *DAPI* forecasts with different lead times (in 16-day intervals). Squares on each line represent the median value for each forecasting model. We present *NRMSE* in the form of 1-*NRMSE* so that the optimal value corresponds to the dashed red line at 1.

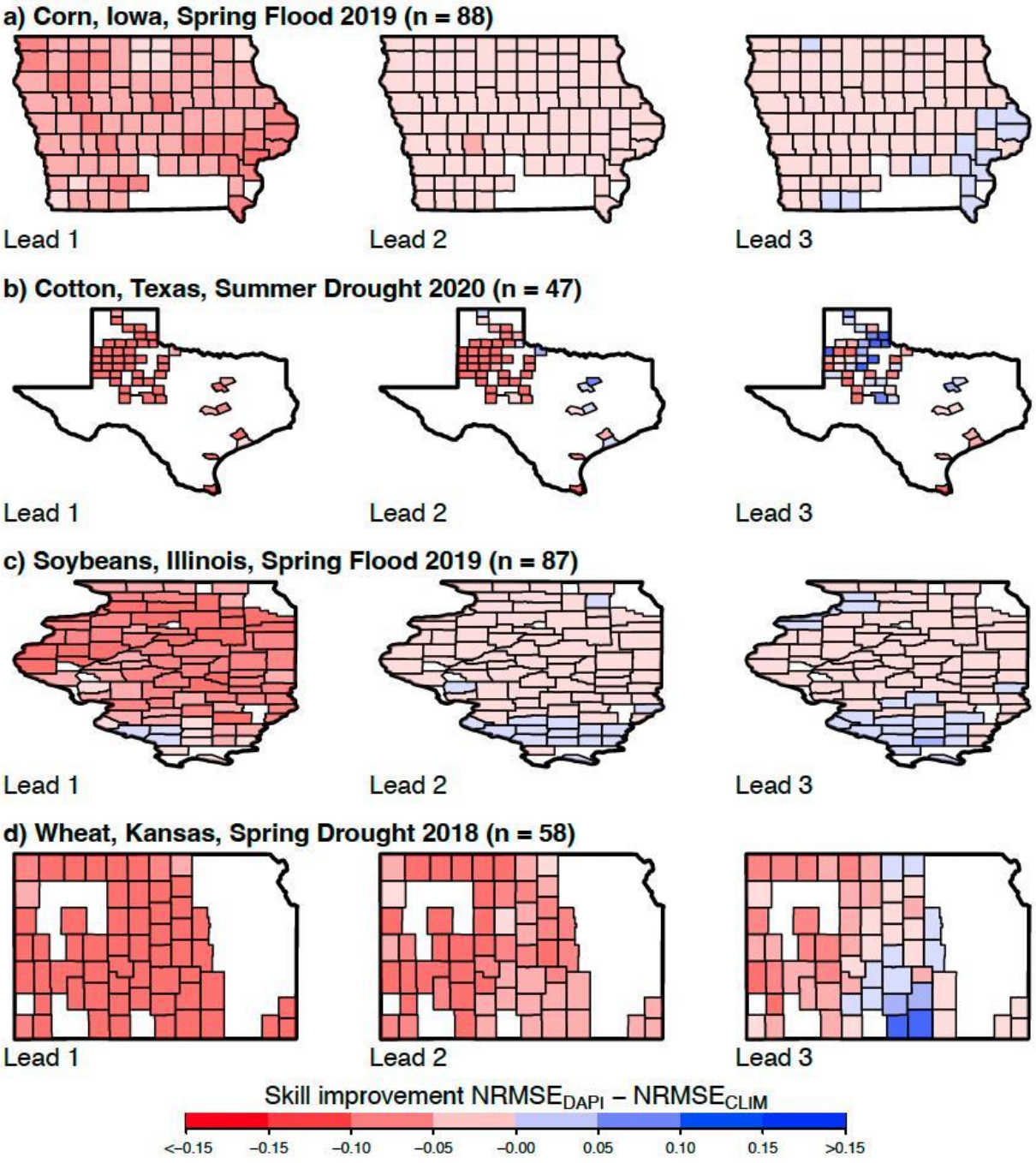

529

530 **Figure 3.** Spatial skill improvement ($NRMSE_{DAPI} - NRMSE_{CLIM}$) at the county level during
531 disturbance years for (a) corn in Louisa County, Iowa, during 2019; (b) cotton in Lynn County,
532 Texas, during 2020; (c) soybeans in Will County, Illinois, during 2019; and (d) wheat in Morton
533 County, Kansas, during 2018. *NRMSE* values were calculated as the average across grid cells
534 within each county.

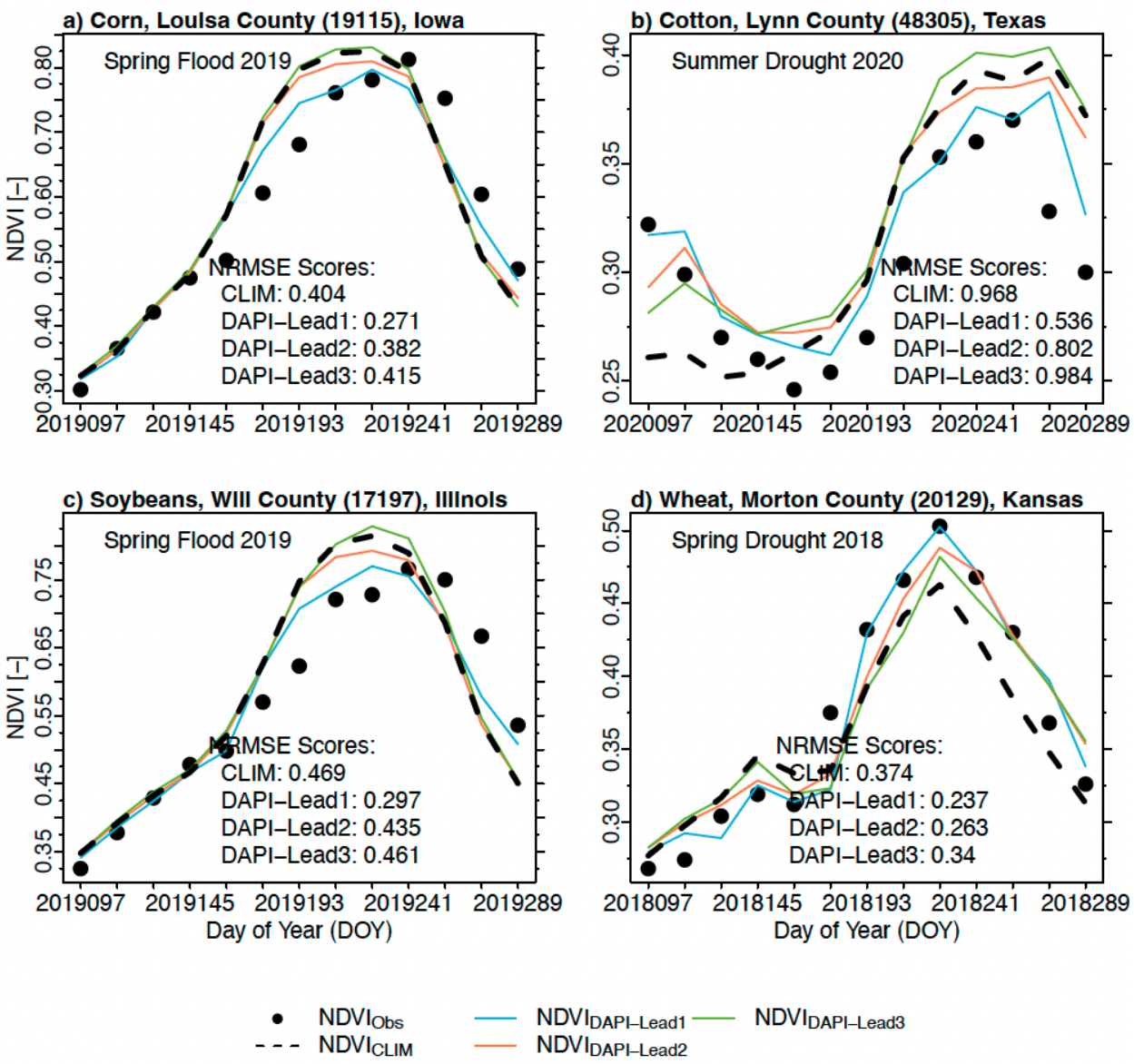

Figure 4. Temporal dynamics of NDVI vegetation health during disturbance years for (a) corn in Louisa County, Iowa, during 2019; (b) cotton in Lynn County, Texas, during 2020; (c) soybeans in Will County, Illinois, during 2019; and (d) wheat in Morton County, Kansas, during 2018. The top left legends denote the times when disturbances occurred. NRMSE was calculated for each specific disturbance year with respect to the climatological *CLIM* and three forecasted NDVI lead times (in 16-day intervals).